

2000 species of Paleozoic stromatoporoids (36). Compared to their Satonda counterparts, the Paleozoic stromatoporoids are characterized by generally thicker growth increments and more regular textures that sometimes show almost perfect superposition of pillars and columns. This texture could have been caused by a larger temporal and spatial persistence of regular fluctuations in the Paleozoic seas compared to the hydrochemically less stable and geologically short-lived Satonda Crater Lake.

Stromatoporoids apparently survived the Frasnian-Fammenian crisis and became extinct during the lowermost Carboniferous (Strunian). Their disappearance has been mostly attributed to ocean cooling or meteorite impact (37). From our studies on Satonda stromatolites we suggest that a worldwide decrease in alkalinity and in carbonate mineral supersaturation following the Fammenian oceanic turnover (38) may better account for the fading of stromatoporoid stromatolites from the late Paleozoic geological record.

REFERENCES AND NOTES

1. A. Goldfuss, *Petrefacta Germaniae*, vol. I (Arnz, Düsseldorf, 1826).
2. J. Kaźmierczak, *Palaeontology* 17, 341 (1974).
3. R. A. Wood, *Spec. Pap. Palaeontol.* 37, 1 (1987); ———, J. Reitner, R. R. West, *Lethaia* 22, 85 (1989).
4. O. Kühn, in *Handbuch der Paläozoologie*, O. H. Schindewolf, Ed. (Borntraeger, Berlin, 1939), vol. 2A, pp. 3–68; E. Flügel, *Palaeontol. Z.* 49, 369 (1975).
5. Y. Dehorne, *Mém. Serv. Explication Carte Géol. Détaill. France* (1920); H. Yabe and T. Sugiyama, *Sci. Rep. Tohoku Imp. Univ. Sendai Ser.* 2 14, 135 (1935); R. G. S. Hudson, *Palaeontology* 2, 180 (1960).
6. R. A. Wood and J. Reitner, *Palaeontology* 29, 469 (1986); J. Wendt, *Neues Jahrb. Geol. Palaeontol. Abh.* 150, 111 (1975).
7. H. Nestor, *Lethaia* 14, 21 (1981); K. Mori, *Stockholm Contrib. Geol.* 37, 167 (1982); O. V. Bogoyavlenskaya, *Stromatoporaty Paleozoya* (Nauka, Moscow, 1984).
8. W. D. Hartman and T. E. Goreau, *Symp. Zool. Soc. London* 25, 205 (1970); C. W. Stearn, *Lethaia* 5, 369 (1972).
9. J. Kaźmierczak, *Nature* 264, 49 (1976).
10. ———, *Acta Palaeontol. Pol.* 25, 243 (1980); ——— and W. E. Krumbein, *Lethaia* 16, 207 (1983).
11. R. Riding and S. Kershaw, *Nature* 268, 178 (1977); C. T. Scrutton, in *The Origin of Major Invertebrate Groups*, M. R. House, Ed. (Academic Press, London, 1979), pp. 167–207; C. Monty, in *Phanerozoic Stromatolites*, C. Monty, Ed. (Springer, Berlin, 1981), pp. v–viii.
12. S. Kempe and J. Kaźmierczak, *Chem. Geol.* 81, 299 (1990).
13. $\delta^{13}\text{C} = [(^{13}\text{C}_{\text{sample}}/^{12}\text{C}_{\text{sample}})/(^{13}\text{C}_{\text{PDB}}/^{12}\text{C}_{\text{PDB}})]1000$, where PDB is the Pee Dee Belemnite standard.
14. The saturation index (SI) is defined as $\log [(IAP)/K_{\text{mineral}}]$, that is for calcite (Cc): $\log \{([Ca^{2+}][CO_3^{2-}]/K_{\text{Cc}})\}$; IAP = ion activity product.
15. L. N. Plummer, B. F. Jones, A. H. Truesdell, *U.S. Geol. Surv. Water Res. Invest. Pap.* 76-13 (1976; revised 1978, 1984).
16. G. Müller, G. Irion, U. Förstner, *Naturwissenschaften* 59, 158 (1972); R. L. Folk, *J. Sediment. Petrol.* 44, 40 (1974).
17. R. Rippka, J. W. Waterbury, R. Y. Stanier, in *The Prokaryotes*, M. P. Starr et al., Eds. (Springer, Berlin, 1981), vol. 1, pp. 247–256.

18. R. J. Horodyski and S. Vonder Haar, *J. Sediment. Petrol.* 45, 894 (1975); W. E. Krumbein and C. Giele, *Sedimentology* 26, 593 (1979); C. J. R. Braithwaite, J. Casanova, T. Frevert, B. A. Whitton, *Palaeogeogr. Palaeoclimatol. Paleocool.* 69, 145 (1988).
19. W. E. Krumbein and Y. Cohen, in *Fossil Algae*, E. Flügel, Ed. (Springer, Berlin, 1977), pp. 37–56; W. E. Lyons et al., *Geology* 12, 623 (1984).
20. K. Simkiss, in *Biominingalization in Lower Plants and Animals*, B. S. C. Leadbeater and R. Riding, Eds. (Clarendon, Oxford, 1986), pp. 19–37; S. Kempe and J. Kaźmierczak, in *Facets of Modern Biogeochemistry*, V. Ittekkot, S. Kempe, W. Michaelis, A. Spitz, Eds. (Springer, Berlin, 1990), pp. 252–275.
21. W. E. Krumbein, in *Biogeochemical Cycling of Mineral-Forming Elements*, P. A. Trudinger and D. J. Swaine, Eds. (Elsevier, Amsterdam, 1979), pp. 47–68; A. Pentecost, *Geomicrobiol. J.* 4, 285 (1985); A. Pentecost and J. Bauld, *ibid.* 6, 129 (1988).
22. J. J. Galloway and J. St. Jean, Jr., *Bull. Am. Paleontol.* 43, 5 (1961).
23. T. E. Bolton, *Geol. Surv. Can. Bull.* 379, 17 (1988).
24. J. J. Galloway, *Bull. Am. Paleontol.* 37, 345 (1957).
25. H. E. Nestor, *Ordovician and Llandoveryan Stromatoporoidea of Estonia* (Valgus, Tallinn, 1964).
26. B. D. Webby, *Palaeontology* 12, 637 (1969).
27. C. W. Stearn, *J. Paleontol.* 62, 411 (1988).
28. D. Y. Dong, *Acta Palaeontol. Sin.* 12, 280 (1964).
29. M. R. Walter, in *Earth's Earliest Biosphere*, J. W. Schopf, Ed. (Princeton Univ. Press, Princeton, 1983), pp. 187–213.
30. J. Casanova, *Sci. Géol. Bull.* 40, 135 (1987); C. Hilaire-Marcel and J. Casanova, *Palaeogeogr. Palaeoclimatol. Palaeoecol.* 58, 155 (1987).
31. D. K. Richter, *Sedimentology* 19, 211 (1972).
32. R. A. Henderson, *J. Sediment. Petrol.* 54, 1138 (1984).
33. L. F. Laporte, Ed., *Soc. Econ. Paleontol. Mineral. Spec. Publ.* 18 (1974); D. F. Toomey, Ed., *ibid.* 30, (1981).
34. T. D. Brock, *Science* 179, 480 (1973).
35. W. B. N. Berry and P. Wilde, *Am. J. Sci.* 278, 257 (1978); P. Wilde and W. B. N. Berry, *Palaeogeogr. Palaeoclimatol. Palaeoecol.* 48, 143 (1984); W. T. Holser, M. Magaritz, J. Wright, in *Global Bio-Events*, O. Walliser, Ed. (Springer, Berlin, 1986), pp. 63–74; J. Wright, H. Schrader, W. T. Holser, *Geochim. Cosmochim. Acta* 51, 631 (1987).
36. E. Flügel and E. Flügel-Kahler, in *Fossilium Catalogus*, I. F. Westphal, Ed. (Jung, Gravenhage, 1968), pp. 1–681.
37. P. Copper, *Geology* 14, 835 (1986); C. W. Stearn, *ibid.* 15, 677 (1987); D. J. McLaren, *ibid.* 13, 170 (1985).
38. H. H. J. Geldsetzer, W. D. Goodfellow, D. J. McLaren, M. J. Orchard, *Geology* 15, 393 (1987); U. Brand, *Palaeogeogr. Palaeoclimatol. Palaeoecol.* 76, 311 (1989).
39. We thank G. Landmann, A. Lipp, Y. Surachman, and D. Susanto for field assistance. The paper has been reviewed by H. K. Wong, W. E. Krumbein, and A. Nissenbaum. Supported by the German Federal Ministry of Research and Technology, Polish Academy of Sciences, and a fellowship from the A. V. Humboldt Foundation (to J.K.). The paper is a contribution to the IGCP Project No. 261, "Stromatolites."

15 May 1990; accepted 22 August 1990

Simulation of Tsunamis from Great Earthquakes on the Cascadia Subduction Zone

MAX K.-F. NG, PAUL H. LEBLOND,* TAD. S. MURTY

Large earthquakes occur episodically in the Cascadia subduction zone. A numerical model has been used to simulate and assess the hazards of a tsunami generated by a hypothetical earthquake of magnitude 8.5 associated with rupture of the northern sections of the subduction zone. Wave amplitudes on the outer coast are closely related to the magnitude of sea-bottom displacement (5.0 meters). Some amplification, up to a factor of 3, may occur in some coastal embayments. Wave amplitudes in the protected waters of Puget Sound and the Strait of Georgia are predicted to be only about one fifth of those estimated on the outer coast.

THE CASCADIA SUBDUCTION ZONE IS the area where the Juan de Fuca plate and smaller adjacent plates slip below the North American continent (Fig. 1). The possibility of a massive earthquake in this area has recently been recognized (1). A seismic sea wave, or tsunami, would be a major risk associated with such an event. In this report, we present calculations that quantify this risk and allow identification of the factors that would determine flooding levels along the adjacent coast.

A critical element in tsunami modeling is the nature of the initial sea-level displacement

that starts the wave. Because the rupture takes place on a time scale that is short compared to the response time of the ocean waters, the sea-surface displacement, which causes the tsunami, is practically identical to that of the sea bottom. Geophysical arguments (2) suggest that a vertical uplift of 5 m of the ocean bottom along the deformation front, decreasing linearly to zero at the coast line, is possible during a large earthquake. We have modeled only the rupture of the northern sections of the Cascadia subduction zone (north of 48°N). A maximum earthquake magnitude of 8.2 is estimated for rupture of each of the Winona and Explorer segments and of about 8.5 for simultaneous rupture of all segments north of 48°N (Fig. 1).

Tsunami propagation from an impulsive

M. K.-F. Ng and P. H. LeBlond, Department of Oceanography, University of British Columbia, Vancouver, BC Canada V6T 1W5.
T. S. Murty, Institute of Ocean Sciences, Post Office Box 6000, Sidney, BC Canada V8L 4B2.

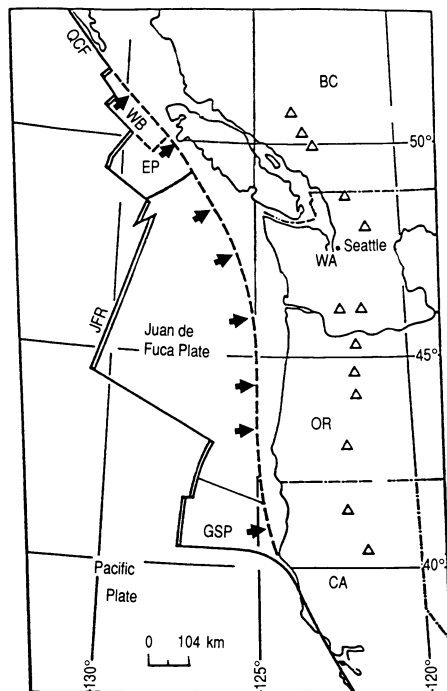


Fig. 1. Schematic view of crustal plates in the northeast Pacific area. The deformation front where the Cascadia subducting segments (Winona Block, Explorer Plate, Juan de Fuca Plate, and Gorda South Plate) slip under North America is shown as a dashed line; it follows approximately the 2000-m depth contour. Tsunami generation by sea-bottom uplift north of 48°N is modeled here. QCF, Queen Charlotte fault; WB, Winona block; EP, Explorer Plate; JFR, Juan de Fuca Ridge; GSP, Gorda South Plate. Triangles indicate cascade volcanoes.

source is well modeled by the shallow-water equations (3). The problem is considered on a plane tangent to the earth's surface (the f -plane); the curvature of the earth can be ignored because of the limited extent of the area considered (4). The governing equations for volume and momentum conservation are

$$\eta_t + [(H + \eta)u]_x + [(H + \eta)v]_y = 0 \quad (1)$$

$$u_t + uu_x + vv_y - fv = -g\eta_x \frac{-Ku(u^2 + v^2)^{1/2}}{(H + \eta)} \quad (2)$$

$$v_t + uv_x + vv_y + fu = -g\eta_y \frac{-Kv(u^2 + v^2)^{1/2}}{(H + \eta)} \quad (3)$$

where u and v are orthogonal velocity components in the x and y directions in the horizontal plane; f is the Coriolis parameter, g is the acceleration due to gravity, H is the mean water depth, η is the deviation of the sea surface from its equilibrium level, and K is a bottom friction coefficient. Subscripts x , y , and t indicate differentiation with respect to spatial coordinates and time.

Calculations were performed in two rectangular finite-difference grids (A and B, Fig. 2 inset). The coarse outer grid has a 5-km by 5-km mesh size and includes the deep ocean and the continental shelf area; a finer, 2-km by 2-km mesh grid was used to represent the coastal Straits of Juan de Fuca and Georgia and Puget Sound (5, 6). The numerical scheme used in both grids was an explicit one-sided difference scheme in space and time; an Arakawa C -type calculation scheme

was used that had already been well tested for the modeling of tsunamis, tides, and storm surges (7). Radiation boundary conditions were applied on the open boundaries, and the model was tested for spurious reflections. A uniform bottom friction coefficient of 0.0025 was used in the coarse-grid model; in the fine-grid model, higher values were used in a number of shallow and narrow channels (6). Matching conditions between the two grids were examined to determine sensitivity to details of the matching configuration. Values in the coarse grid were smoothed through an overlap area to provide driving conditions for the fine-grid model.

A typical history of sea-level displacement is illustrated in Fig. 3 for the earthquake caused by the simultaneous rupture of the Winona and Explorer segments. In the model, the initial triangular pulse of the displacement rapidly disperses and decays seaward. The largest sea-level perturbations were observed on the continental shelf, where sea-level oscillations continued much longer than offshore.

Detailed time histories of sea-level displacements generated by the rupture of all segments north of 48°N (Fig. 4) show that the peak of the first tsunami wave reaches the coast of Vancouver Island within about one-half hour. At Victoria, the first wave arrives slightly more than 2 hours after the earthquake; for Vancouver and Seattle, the delay is closer to 4 hours. At a solid wall, in an ocean of uniform depth, a wave front such as that generated by the nearly plane deformation front would double in amplitude because of the superposition of incoming and reflected waves. In practice, reflection takes place mostly at the continental slope, and wave amplitudes at the shore are generally comparable to the maximum uplift of the sea floor rather than being twice as large. The configuration of the continental shelf as well as the indentations and inlets of the coast account for the precise values of local sea-level variations. Narrow shelf areas, such as near Cape St. James, exhibit typical oceanic high-frequency response. Where the shelf is broader, amplification and low-fre-

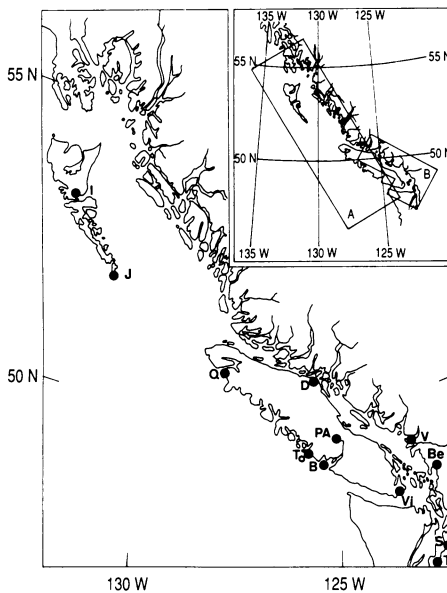
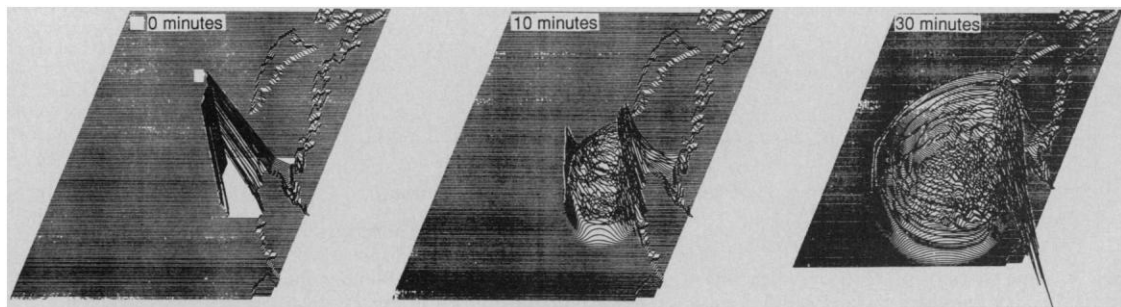


Fig. 2. Grid locations and points at which time series of sea level are shown in Fig. 4. I, Queen Charlotte City; J, Cape St. James; Q, Quatsino Sound; D, Discovery Passage; PA, Port Alberni; B, Barkley Sound; To, Tofino; V, Vancouver Harbor; V, Victoria; Be, Bellingham; S, Seattle; T, Tacoma.

Fig. 3. Perspective views of sea-level displacement at successive times following the earthquake due to rupture of the Winona Block alone. Vertical scale is given by the 5-m initial vertical uplift at the deformation front, the western edge of the triangular source function at time $t = 0$.



quency resonance occur, for example, near the mouth of Quatsino Sound. The strongest amplification occurs in Alberni Inlet, a narrow fjord on the west coast of Vancouver Island already well known for its resonant response in earlier tsunamis (7). A special one-dimensional model was used to represent Alberni Inlet, at the head of which flooding levels of up to 16 m were calculated (Fig. 5). The amplification factor of 3.0 between Barkley Sound at the mouth (B in Fig. 2) and Port Alberni (PA) at the head of the inlet is consistent with that observed or calculated by others (8) and with the notion that the body of water in the inlet responds as a quarter-wave oscillator with a period of about 85 minutes.

At the mouth of the Strait of Juan de Fuca (D in Fig. 2), the simulated tsunami amplitude is about 2 m. The wave propagates through that deep (300 m) strait without much loss in amplitude past Victoria and Bellingham, beyond which it penetrates into Puget Sound to the south and the Strait of Georgia to the north. A considerable amount of energy is lost through the narrow and shallow passages connecting these straits to the Strait of Juan de Fuca: simulated tsunami amplitudes are reduced to 1 m or

less by the time the wave reaches Seattle and Tacoma. Geometric and bathymetric details are again seen to be important in determining local response. Vancouver Harbor, for example, behaves like a Helmholtz resonator with a period of about 3 hours (9). The sensitivity of the results to the local geometry suggests that more accurate modeling at a higher level of resolution is needed.

Nonlinearity is not important in our results. Sea-level displacements obtained from a linearized form of Eqs. 1 to 3 are nearly indistinguishable from those described above. We have also found that a doubling of source strength results nearly in a doubling of the response. Tsunamis generated by the rupture of only the northern Juan de Fuca section or only the Winona and Explorer sections of the subduction zone have also been computed. Because of the elongated form of the source, the near-field tsunami response in our model is due mainly to nearby segments. Removal of the northerly (Winona and Explorer) segments affects principally the results for nearby coastal regions; amplitudes in the Strait of Juan de Fuca are not changed appreciably (only a few centimeters).

A tsunami would of course be superimposed upon the tides, which in the area considered have a range of up to 5 m (10). A positive sea-level displacement at low tide

would be of little consequence, but our results show that oscillations associated with a tsunami could persist for at least a tidal cycle, so that extreme displacements above and below sea level are likely to combine both tsunami and tidal effects. The former lead to flooding, which is the most significant tsunami effect; the latter to abnormally low sea levels, which may cause navigational problems. In both extreme cases, areas normally not exposed to wave action may find themselves subjected to destructive erosion.

Extensive flooding of low-lying areas may take place, especially on the outer coast. More precise evaluation of flooding risks requires high-resolution modeling of the local response, which includes wetting of normally dry areas. It is clear that a wooded patch, or a combination of fields, canals, roads and houses, does not behave like an ocean floor and that a more complex modeling procedure is needed to take into account the detailed frictional and storage properties of the flooded area (11).

Finally, the calculated wave amplitudes are of course a function of that of the sea-floor displacement, which remains to be improved from a better understanding of the tectonics. In spite of this uncertainty, our model provides a useful link between the generating event and its effects on the shore. A locally large tsunami may arise from rupture of only a small part of the Cascadia deformation front, in a large but not implausible earthquake.

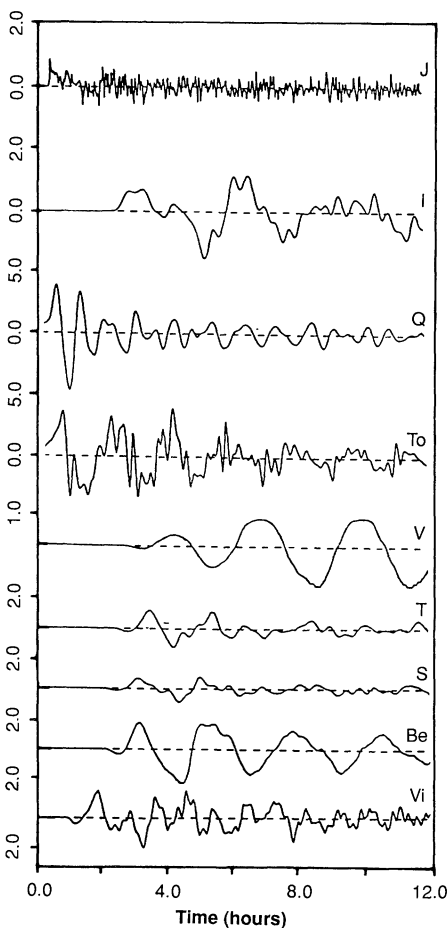


Fig. 4. Time series of sea-level displacements at selected points; locations shown on Fig. 2.

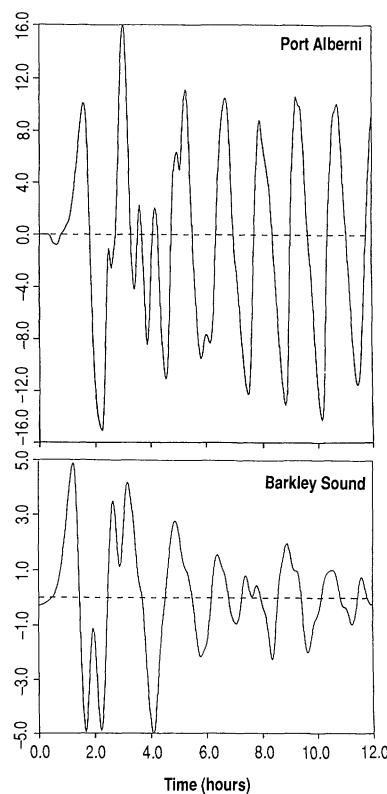


Fig. 5. Resonant response in Alberni Inlet, showing time series of sea-level displacement at mouth of the inlet (Barkley Sound, B in Fig. 2) and at the head (Port Alberni, PA in Fig 2).

REFERENCES AND NOTES

1. T. H. Heaton and H. Kanamori, *Bull. Seismol. Soc. Am.* **74**, 933 (1984); T. H. Heaton and S. H. Hartzell, *Science* **236**, 162 (1987).
2. The bottom-deformation model is based on the work of G. C. Rogers [*Can. J. Earth Sci.* **25**, 844 (1988)] and H. Dragert and G. C. Rogers [*Geos* **17**, 5 (1988)] and was discussed with these authors. Rogers also gives estimates of earthquake magnitudes, on the basis of an empirical relationship of L. Ruff and H. Kanamori [*Phys. Earth Planet. Inter.* **23**, (1980)].
3. L. S. Hwang and D. Divoky, *J. Geophys. Res.* **75**, 6802 (1970); H. G. Ramming and Z. Kowalik, *Numerical Modelling of Marine Hydrodynamics* (Elsevier, Amsterdam, 1980); Z. Kowalik and T. S. Murty, *Geophys. Res. Lett.* **12**, 1243 (1984).
4. The error associated with neglecting the curvature of the earth was estimated at a maximum of 6% of calculated wave amplitudes.
5. The coarse grid was adapted from D. S. Dunbar, P. H. LeBlond, T. S. Murty, *Prog. Oceanogr.*, in press; a 300-km seaward extension at a fixed depth of 2700 m was annexed to that grid to minimize the effect of open-boundary reflections. The finer grid is that used in (6).
6. P. B. Crean, T. S. Murty, J. Stronach, *Mathematical Modelling of Tides and Estuarine Circulation* (Springer, New York, 1988).
7. T. S. Murty, *Can. Bull. Fish. Aquat. Sci.* **212**, 1 (1984).
8. L. Boilard, in *Tsunamis in the Pacific Ocean*, W. M. Adams, Ed. (East-West Center, Honolulu, 1970), chap. 8, pp. 165-190.
9. W. D. Baines, in *Proceedings of the 6th Coastal Engineering Conference, Miami Beach*, J. W. Johnson, Ed. (Council on Wave Research, The Engineering

- Foundation, New York, (1957), pp. 545–561.
10. B. B. Parker, NOAA (Natl. Oceanic Atmos. Adm.) Tech. Rep. 69 (1977).
11. Some progress has been made in that direction in models of storm-surge phenomena, as reported in (7).
12. We thank D. S. Dunbar for letting us use his

digitized bathymetry of the west coast of Vancouver Island and F. Henry for advice on radiation boundary conditions. This research was sponsored by the Natural Sciences and Engineering Research Council of Canada.

7 May 1990; accepted 1 September 1990

Exploitation of Herbivore-Induced Plant Odors by Host-Seeking Parasitic Wasps

T. C. J. TURLINGS, J. H. TUMLINSON,* W. J. LEWIS

Corn seedlings release large amounts of terpenoid volatiles after they have been fed upon by caterpillars. Artificially damaged seedlings do not release these volatiles in significant amounts unless oral secretions from the caterpillars are applied to the damaged sites. Undamaged leaves, whether or not they are treated with oral secretions, do not release detectable amounts of the terpenoids. Females of the parasitic wasp *Cotesia marginiventris* (Cresson) learn to take advantage of those plant-produced volatiles to locate hosts when exposed to these volatiles in association with hosts or host by-products. The terpenoids may be produced in defense against herbivores but may also serve a secondary function in attracting the natural enemies of these herbivores.

MOST STUDIES ON THE SIGNIFICANCE of herbivore-induced production of secondary metabolites in plants focus on the direct ecological interactions between plants and the herbivores that feed on them (1–3). Only a few investigators (4–6) have suggested active interactions between herbivore-damaged plants and the third trophic level of insect parasitoids and predators. There are many examples of these insects being attracted to plant odors (7), but only recently have studies indicated an active involvement of plants (5, 6). Dicke and co-workers presented the first convincing evidence for an active release of volatiles by herbivore-infested plants that attract natural enemies of the herbivorous attackers (6). As yet, no herbivore-specific factor that induces characteristic changes in plants, used by foraging entomophagous insects, has been pinpointed.

It is common that parasitic wasps learn to respond to specific odors that are associated with their hosts (8). The often observed flexibility in these responses has been attributed to the variability in space and time of reliable cues that may best guide the wasps to available hosts (9). Their ability to learn should allow parasitoids to distinguish among odors of plants with different types

of damage, thus enabling them to focus on plants damaged by potential hosts. Chemical responses evoked in plants by herbivorous hosts may therefore play an important role in host-habitat location by parasitoids. We report that herbivore-inflicted injury induces plants to release volatile terpenoids. The plant response is greatly enhanced by the oral secretions of caterpillars and is exploited by the parasitic wasp *C. marginiventris*, which uses the terpenoids as cues to locate hosts.

In flight tunnel trials, females of the parasitoid *C. marginiventris* are attracted to the

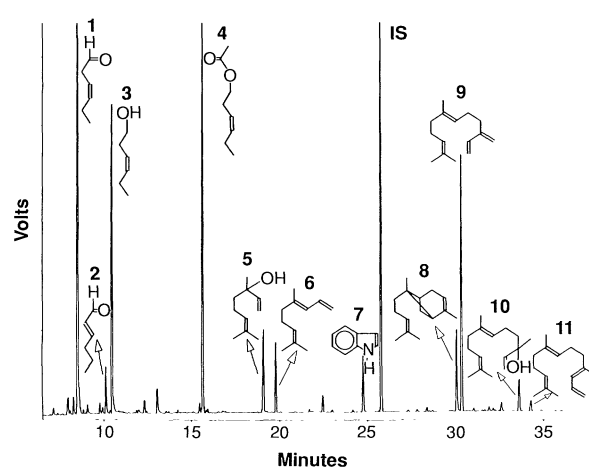
odors emanating from a complex of host larvae feeding on corn (*Zea mays* L., var. "Ioana sweet corn") seedlings (10). Of the three main components of a complete plant-host complex, the damaged plants, and not the host larvae or their feces, are the main source of the volatiles that attract the parasitoid (10).

Volatiles from a complete plant-host complex consisting of beet armyworm larvae (BAW), *Spodoptera exigua* (Hübner), that were feeding on corn seedlings inside an all-glass collection system (11) were collected in traps containing Super Q adsorbent (12). Gas chromatographic analyses of methylene chloride washes of the traps revealed the consistent presence of eleven compounds (Fig. 1). The first four most volatile compounds were identified as leafy aldehydes, an alcohol, and an acetate, commonly found in the leaves of many plants (13). The remaining compounds were, except for indole, all terpenoids.

All the identified compounds are released by the caterpillar-damaged seedlings and not by the caterpillars themselves nor by something in their feces or other by-products (14). Additional volatile collections, however, revealed that the larger terpenoids, particularly α -trans-bergamotene, (*E*)- β -farnesene, and (*E*)-nerolidol, were only released by leaves that had been damaged by caterpillars for several hours. Plants subjected to caterpillar damage for 2 hours released the larger terpenoids only in minute amounts immediately afterward. The following day, however, large amounts of these compounds could be detected (Fig. 2).

Fast growing plants like corn invest much of their energy in growth and little in de-

Fig. 1. A chromatographic profile of the volatiles collected from a complex of BAW caterpillars feeding on corn seedlings. The identified compounds are 1, (*Z*)-3-hexenal; 2, (*E*)-2-hexenal; 3, (*Z*)-3-hexen-1-ol; 4, (*Z*)-3-hexen-1-yl acetate; 5, linalool; 6, (3*E*)-4,8-dimethyl-1,3,7-nonatriene; 7, indole; 8, α -trans-bergamotene; 9, (*E*)- β -farnesene; 10, (*E*)-nerolidol; and 11, (3*E*,7*E*)-4,8,12-trimethyl-1,3,7,11-tridecatetraene. For this particular collection, 15 early third instar caterpillars were allowed to feed on three 2-week-old greenhouse-grown corn seedlings. After 14 hours of feeding, the seedlings together with the caterpillars were transferred into the collection apparatus (11). Volatiles were collected for 2 hours in traps containing 25 mg of Super Q adsorbent (12). The traps were then extracted with 200 μ l of methylene chloride and an internal standard (IS) in 50 μ l of methylene chloride (*n*-nonyl-acetate, 20 ng/ μ l) was added. Of the extract 2.5 μ l was injected onto a Quadrex methyl silicone column (50 m by 0.25 mm inside diameter, 0.25 μ m film) inside a Varian model 3700 gas chromatograph. Temperature program: 50°C, rate 5°C/min to 180°C. Compounds were identified by mass spectroscopy and, where necessary, by NMR spectroscopy. Their identities were confirmed with synthetic versions of the candidate compounds (14).



T. C. J. Turlings and J. H. Tumlinson, Insect Attractants, Behavior and Basic Biology Research Laboratory, Agricultural Research Service, U.S. Department of Agriculture, Gainesville, FL 32604.

W. J. Lewis, Insect Biology and Population Management Research Laboratory, Agricultural Research Service, U.S. Department of Agriculture, Tifton, GA 31793-0748.

*To whom correspondence should be addressed.